Cell, Vol. 80, 651–660, February 24, 1995, Copyright © 1995 by Cell Press

Crystal Structure of the Replication Terminator Protein from B. subtilis at 2.6 Å

Dirksen Eli Bussiere, Deepak Bastia, and Stephen W. White
The Department of Microbiology
and The Program in Cell and Molecular Biology
Duke University Medical Center
Durham, North Carolina 27710

Summary

The crystal structure of the replication terminator protein (RTP) of B. subtilis has been determined at 2.6 Å resolution. As previously suggested by both biochemical and biophysical studies, the molecule exists as a symmetric dimer and is in the α+β protein-folding class. The protein has several uncommon features, including an antiparallel coiled-coil, which serves as the dimerization domain, and both an α-helix and a β-ribbon suitably positioned to interact with the major and minor grooves of B-DNA. A site has been identified on the surface of RTP that is biochemically and positionally suitable for interaction with the replication-specific helicase. Other features of the structure are consistent with the polar contrahelicase mechanism of the protein. A model of the interaction between RTP and its cognate DNA is presented.

Introduction

Over the past decade, structural biology has provided crucial insights into the understanding of genetic mechanisms at the molecular level (Ollis and White, 1987; Steitz, 1990). However, relatively little structural information is available on the process by which DNA replication is terminated within defined regions on the chromosome. DNA replication can be separated into three distinct steps: initiation, elongation, and termination. In most prokaryotic systems, it is now clear that the termination step does not occur at random positions on the genome, but is instead a precisely controlled event that occurs in a defined region of the circular DNA. The process has been particularly well studied in Escherichia coli (Kuempel et al., 1977; MacAllister et al., 1990), Bacillus subtilis (Weiss and Wake, 1984; Lewis et al., 1989, 1990), and the autonomously replicating plasmid R6K (Bastia et al., 1981), and the sequence of events that takes place in these systems is rather similar. The termination site comprises two adjacent sequences that are imperfect inverted repeats, and these are the targets for site-specific DNA-binding proteins known as terminator proteins. The protein–DNA complex will either arrest or permit the passage of an approaching replication fork depending on the direction of approach, and the arrangement ensures that the two forks generated at the origin fuse precisely within the termination site. We have shown that the terminator protein operates by blocking, in a polar fashion, the ATP-dependent unwinding of DNA by the replicative helicase (DnaB in E. coli). We have suggested the term "contrahelicase" to describe this unique property (Khatri et al., 1989).

Figure 1 shows the B. subtilis imperfect repeat region. It has an overall size of 154 bp and comprises the two repeat regions IRI (47 bp) and IRII (48 bp), separated by 59 bp (Lewis et al., 1990; Smith and Wake, 1992). The terminator protein, known as the replication terminator protein (RTP; Lewis et al., 1990; Smith and Wake, 1992), has a molecular weight of 14,500 daltons (122 amino acids) per monomer and is encoded by the *rtp* gene immediately adjacent to the imperfect repeat region. RTP has been shown to exist as a functional dimer both in solution and when bound to DNA (Lewis et al., 1990; Kralicek et al., 1993), and it has no obvious sequence similarity to any other known DNA-binding protein. Two dimers of RTP bind to each inverted repeat, and the binding of each is centered on an 8 bp "direct repeat" that exists within a larger 20–21 bp sequence identified by DNaseI footprinting studies (Lewis et al., 1990; Lewis and Wake, 1991).

Interestingly, RTP can serve as an effective polar contrahelicase in E. coli (Kaul et al., 1994; Sahoo et al., 1994) even though, at the molecular level, RTP and the E. coli terminator ter (also known as Tus) appear to be quite dissimilar. There is very little primary sequence similarity between the two proteins (22% identity and a 40% similarity), and ter is much larger (300 amino acids) and functions as a monomer (Sista et al., 1991; Lee and Kornberg, 1992). Experimentally, the RTP/E. coli surrogate system has proven to be invaluable in analyzing the mechanism of RTP (see Discussion).

With a view to understanding the molecular basis of the termination of DNA replication, we have solved the crystal structure of RTP to 2.6 Å. The protein has unique structural characteristics that provide crucial insights into how it accomplishes its biological function. We propose that RTP binds DNA in both the major and minor grooves of its 2-turn recognition sequence, using both α-helices and β-ribbons as recognition elements. A model of the RTP–DNA interaction is presented, and a possible site of interaction with the replication fork helicase is described.

Results

Crystal Structure Determination

The full-length RTP molecule was purified in a biologically active form and crystallized as previously described (Mehta et al., 1992). The crystals belong to the monoclinic space group C2 and contain a dimer in the asymmetric unit. The crystal structure of RTP was solved by the heavy atom multiple isomorphous replacement method combined with solvent flattening, noncrystallographic symmetry averaging, and phase extension, as described in Experimental Procedures. This procedure provided a relatively clean electron density map, and the main and side chains of the RTP molecule were readily fitted into the calculated density. Refinement proceeded smoothly to an R factor

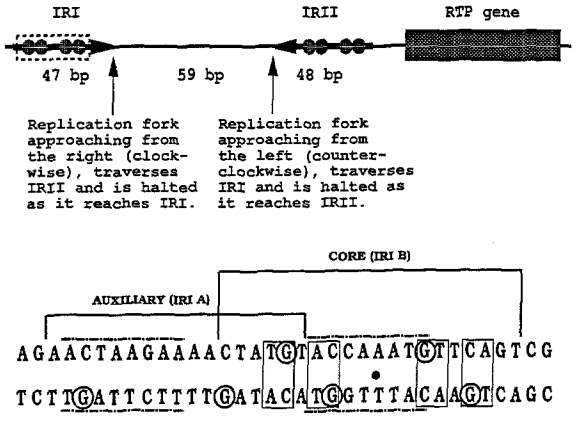

Figure 1. The Inverted Repeat Region of the B. subtilis Replication Terminus

The two repeat regions, IRI and IRII, are represented by arrows, and each bound RTP dimer is shown as a stippled dumbbell. The IRI sequence of strain 168 (boxed) is shown in greater detail below. IRIB is the "core" sequence that binds RTP tightly, and IRIA is the "auxiliary" sequence that binds RTP less tightly. The approximate dyad axis of the core sequence is shown by the black dot, and base pairs that obey this dyad exactly are boxed. The "direct repeats" identified previously in both IRIA and IRIB (Lewis et al., 1990) are bordered by dashed lines. The guanines that have been shown by protection experiments (Sahoo et al., 1994) to contact the bound RTP are circled. Note that both sequences are A/T rich.

of 19.3% at 2.6 Å (for 2σ data from 6.0–2.6 Å), and the root mean square (rms) deviation from ideal geometry is 0.013 Å for bond lengths and 1.80° for bond angles, with good stereochemistry for the backbone torsion angles.

The structure determination was relatively straightforward, with the important exception of the heavy atom derivatives. The search for traditional derivatives proved to be very difficult, and a selenomethionine-substituted (semet-substituted) protein was generated with a view to performing a multiwavelength anomalous dispersion experiment. However, the isomorphous differences from the selenium atoms (two per monomer or four per asymmetric unit) were sufficient to provide good initial phase information without the need to invoke multiwavelength anomalous dispersion. This procedure required that the *rtp* gene be expressed in an E. coli methionine auxotroph under the control of a T7 promoter (see Experimental Procedures).

Representative electron density from the final refined model is shown in Figure 2. Apart from a disordered loop, the extreme N-terminus and a few surface side chains (mostly lysines), the final electron density is well defined for both molecules in the asymmetric unit. The main chain carbonyl groups are clearly visible for almost all the residues. To assess the overall validity of the structure, the local environments of all the amino acids within the RTP dimer were checked using the three-dimensional (3D) profile technique developed by Luthy et al. (1992). The 3D-1D score for appropriately placed amino acids has been shown to vary from 0.2–0.8, and the values in RTP vary between 0.4–0.6.

Overall Structure of RTP

RTP is a dimeric molecule in which only the N-terminal 6 amino acids are completely missing in the electron density and are apparently disordered. RTP belongs to the α+β family of proteins (Levitt and Chothia, 1976), and each monomer contains four α-helices and three β-strands. Proceeding from the disordered N-terminal 6 amino acids, the secondary structural elements are as follows (Figure 3). The first element is the 4-turn α-helix α1 that connects to the 3-turn α-helix α2 via β-strand β1. The next element is the 3-turn α-helix α3 that leads into an antiparallel β-ribbon structure comprising β-strands β2 and β3. The ends of the β-ribbon proximal to the body of the protein combine with β-strand β1 to form a small region of 3-stranded antiparallel β-pleated sheet. The final and most striking feature of the molecule is the C-terminal 8-turn α-helix α4. The connections between these elements are mostly very short, with the exception of α2→α3 and β2→β3. The latter is rather flexible and may have an important functional role (see below).

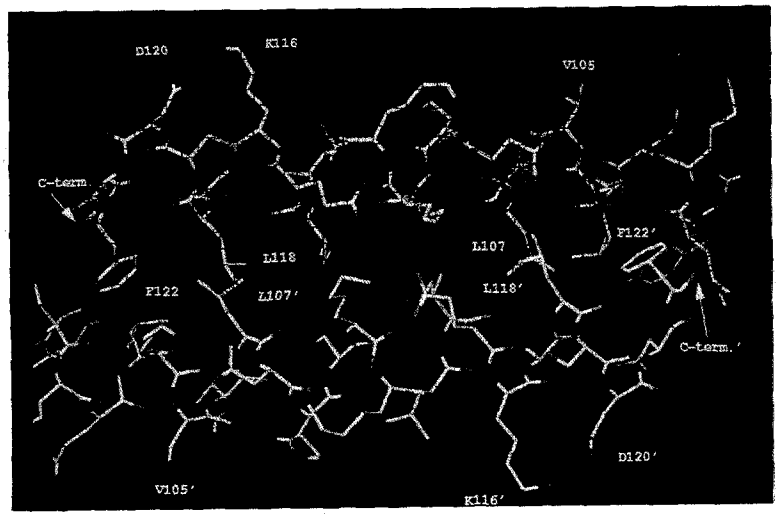

Figure 2. (2Fo-Fc) Electron Density Map of the B. subtilis RTP Calculated with Phases from the Final Refined Model at 2.6 Å

The map is contoured at the 1.5 standard deviation level and shows the antiparallel coiled-coil dimerization region.

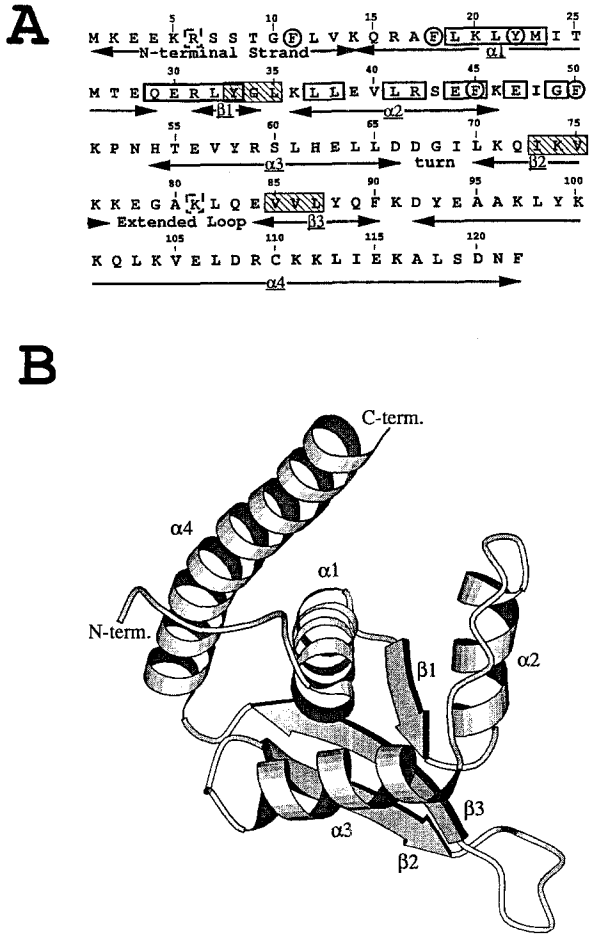

Figure 3. Organization of the RTP Monomer

(A) Primary structure using the one-letter code. Regions of secondary structure are marked with arrows and labeled. Aromatic residues in the hydrophobic core aromatic network are circled. Residues susceptible to clostripain cleavage are shown in a dashed box. Residues in an open box show homology to a region of the B. subtilis DnaB initiator protein. Residues surrounded by a hatched box form the hydrophobic patch proposed to mediate contrahelicase activity by protein–protein interactions.

(B) Cartoon of the structure using MOLSCRIPT (Kraulis, 1991). The N- and C-termini are indicated, and the ribbons and spirals denote α-helices and β-strands, respectively.

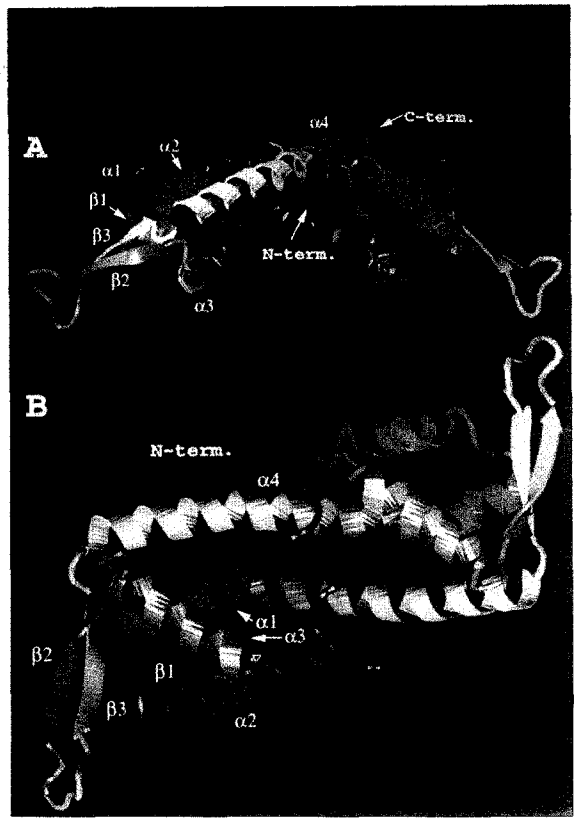

Figure 4. Organization of the RTP Dimer

The ribbon diagrams of the polypeptide backbone were produced by program O (Jones et al., 1991), with spirals and arrows denoting the α-helices and β-strands, respectively. The cartoons are color ramped blue to red, N-terminus to C-terminus, to show the path of the polypeptide chain. Side view (A) and bottom view (B) showing the proposed DNA-binding surface.

Two RTP monomers associate via their long C-terminal α-helices to create the dimer (Figure 4). It has an overall rectangular shape with approximate dimensions of 66 Å × 35 Å × 30 Å. The two subunits are tightly associated; using a water-sized probe of radius 1.6 Å (Lee and Richards, 1971), the loss of accessible surface area upon dimerization is calculated to be 3343 Å^2. The fact that RTP crystallizes with two independent molecules in the asymmetric unit allows us to detect any features of the structure that result from crystal-packing forces. When the two molecules are superimposed, the rms deviation of the main chain and β-carbon atoms is only 0.7 Å. The only major difference between the two is in the flexible loop between β2 and β3, which adopts distinct conformations in each molecule. It should be noted that in solution, the flexible loop is free to adopt different conformations within a dimer. This is not possible in the crystal, in which each dimer is positioned on a crystallographic dyad axis.

Independent solution data on RTP are consistent with the crystal structure. Digestion of RTP with clostripain revealed only two cleavage sites: Arg-6 and Lys-81 (Kralicek et al., 1993). The crystal structure confirms that both are suitably exposed for proteolytic cleavage (see Figure 3A); Arg-6 is within the disordered N-terminal region, and Lys-81 is part of the flexible loop between β2 and β3. In addition, sedimentation equilibrium studies, as well as 2D nuclear magnetic resonance analysis, confirm that RTP exists in solution as a symmetric dimer (Kralicek et al., 1993).

The Dimerization Domain and the Hydrophobic Core

In traversing from its own monomer to its dimeric partner, the long C-terminal helix α4 is involved in three interactions that are crucial to the RTP structure. The proximal third (residues 93–103) has hydrophobic residues on its inner surface that contribute to its own hydrophobic core (Tyr-93 and Tyr-99, Ala-95 and Ala-96, and Leu-103). The majority of the distal two-thirds of α4 associates with the complementary region of α4′ (the prime refers to a dimeric feature)

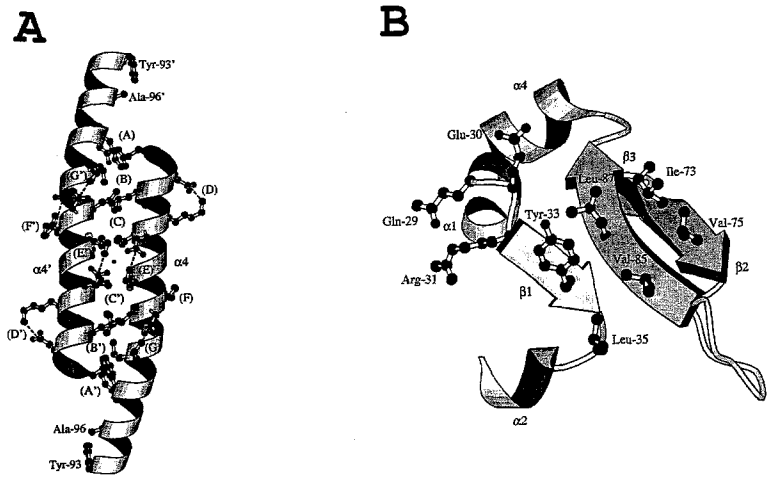

Figure 5. Features of RTP

The diagrams were generated by the MOLSCRIPT program (Kraulis, 1991).

(A) Coiled-coil dimerization region. All the important interactions within the α4/α4′ α-helices are shown. Side chains are shown as balls and sticks. Dashed lines indicate salt bridges. The heptad position ([a]–[g]) of each residue in the coiled-coil is indicated.

Abbreviations: A, Phe-122[b]–(Leu-103′[d′], Lys-104′[e′]); B, Leu-107′[a′]–(Ala-117[d], Leu-118[e]); C, Ile-114[a]–(Cys-110′[d′], Lys-111′[e′]); D, Lys-116–Asp-120; E, Lys-111–Glu-115; F, Glu-106–Arg-109; and G, Lys-104–Asp-108.

(B) Surface region of the RTP monomer proposed to mediate contrahelicase activity by protein–protein interactions. For clarity, only relevant elements of the structure are shown. The region is centered on the exposed surface of the antiparallel 3-stranded β-sheet. Side chains are shown as balls and sticks. Residues 33, 35, 73, 75, 85, and 87 form the hydrophobic patch, while residues 29–33 show homology with the DnaB initiator protein.

to form an antiparallel coiled-coil structure. Finally, a hydrophobic residue at the extreme distal end contributes to the hydrophobic core of the other monomer (Phe-122). This arrangement results in one entire face of α4 being exposed at the "top" of the molecule, and this is reflected in the amphipathic nature of its amino acid sequence (see Figure 3A). The hydrophilic surface is populated with several clear intrahelical salt bridges (Figure 5A) that are known to stabilize exposed α-helices (Scholtz et al., 1993).

The antiparallel coiled-coil region of α4/α4′ is shown in Figure 5A. It conforms to a left-handed superhelical structure with a twist of 70° and a crossing angle of approximately 30°. The interaction of the two α-helices is tighter at the center than at the ends, with an interaxis separation of 9 Å and 11.7 Å, respectively. The contact area between the two α-helices is on the order of 1000 Å^2, which corresponds to a dimerization energy from the hydrophobic effect of approximately 25 kcal/mol (Richards, 1977). Parallel coiled-coils have a distinctive pattern of repeating hydrophobic groups that mediate their interaction according to the "knobs-in-holes" model, first proposed by Crick (1953). The repeat is the so-called heptad, labeled [a]–[g], in which [a] and [d] are hydrophobic and interdigitate at the helical interface (O'Shea et al., 1991; Oas and Endow, 1994). The situation is similar with antiparallel coiled-coils, but the slightly different geometry of the interacting side chains (which always point towards the N-terminus in an α-helix) results in a [a] to [d′]/[e′] interaction (Cusack et al., 1990). This is the pattern observed in RTP (Figure 5A). The four lysines at positions [e]/[e′] might appear to be an anomaly, but it is the aliphatic part of the side chain that is involved in the interaction, while the positively charged end is exposed to solvent. The coiled-coil region lacks the interhelical salt links and hydrogen bonds often seen in other coiled-coils (Pathak and Sigler, 1992).

The majority of the hydrophobic core residues are situated on the inner surfaces of the secondary structure elements, which gives them a distinctly amphipathic character. The one exception is α1, which penetrates through the core and has exclusively hydrophobic residues at its center (see Figures 3a and 3b). Each monomer also donates two hydrophobic core residues to its partner: Phe-11 from the N-terminal strand and Phe-122 from α4. These can be regarded as bona fide dimerization elements of the molecule. A particularly noteworthy feature of the hydrophobic core is the presence of an aromatic network. This network consists of five residues, Phe-11′, Phe-18, Phe-45, Phe-50, and Tyr-22, which are clustered in a relatively small volume of 425 Å^3. The interactions between these aromatic side chains conform to the general principles described by Burley and Petsko (1985). Such networks represent an efficient way of providing protein stability and have been seen in other small DNA-binding proteins, such as λ repressor (Pabo and Lewis, 1982) and HU (Tanaka et al., 1984).

Potential Mode of Interaction with DNA

Any model for the RTP–DNA complex must satisfy three biochemical criteria. First, several independent experiments have clearly shown that RTP binds two turns of DNA (Lewis et al., 1990; Mehta et al., 1992; Langley et al., 1993). In addition, the specificity of binding is maintained throughout this length. Second, the IRIB target site has pseudo 2-fold symmetry (Kralicek et al., 1993) and, like other dimeric DNA-binding proteins (Steitz, 1990), this probably aligns with the dyad axis of the protein. Finally, the model should provide an explanation for the polar functional properties of the RTP–DNA interaction. The "bottom" surface of RTP (opposite the coiled-coil) has three features that are ideally positioned to fulfill these requirements. The dyad-related β-ribbons at the periphery are

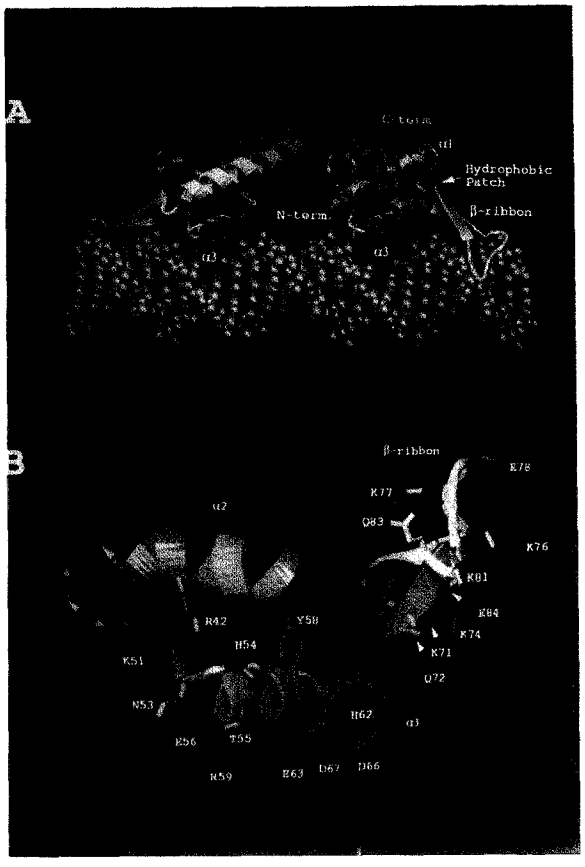

Figure 6. Model of the Interaction between the RTP Dimer and DNA

The cartoons were produced by the O program (Jones et al., 1991), and the backbone is color ramped blue to red, N-terminus to C-terminus.
(A) Complete model of the RTP dimer docked onto standard B-form DNA. Key secondary structural elements and the hydrophobic patch are labeled. The α3 α-helices fit snugly within the major groove, and the N-terminal strands and the β-ribbons run along the minor groove.
(B) Details of the proposed DNA recognition elements of α3 and the β-ribbon. Positively charged side chains are shown in blue, negatively charged side chains are shown in red, and nonpolar side chains maintain the color of that position within the color ramp.

Figure 7. Surface Electrostatic Potential of the RTP Dimer

The electrostatic potential is superimposed on the solvent-accessible surface of RTP calculated using a water probe radius of 1.4 Å. The calculations and representation were performed by the GRASP program (Nicholls and Honig, 1993). The extreme ranges of red (negative) and blue (positive) represent electrostatic potentials of <-7 to $>+7$ k_bT, where k_b is the Boltzmann constant and T is the temperature. White represents nonpolar residues. In the calculations, the pH is 7.0, and the dielectric constants for the solvent and protein are 80 and 2, respectively.
(A) Side view showing the clustering of positive potential at the bottom of the molecule. The proposed DNA-binding surface spans the entire bottom of the molecule. This view corresponds to that in Figure 4A.
(B) Bottom view looking "up" at the α3 α-helices and the proposed DNA-binding surface. The positive potential at the center corresponds to the antiparallel N-terminal β-strands. This view corresponds to that in Figure 4B.

separated by approximately 68 Å or two turns of DNA. Inside these, the dyad-related α-helices α3/α3′ are separated by almost exactly 34 Å or one turn of DNA. Finally, the N-termini associate in an antiparallel fashion at the center of this surface. Therefore, a simple model is that the β-ribbons and the N-termini interact with successive minor or major grooves, and the α3 helices interact with the intervening grooves.

This model was further investigated by computer graphics and RTP–DNA docking exercises using the RTP dimer and a 30-bp model of the core sequence and flanking areas modeled as B-DNA. This docking was performed visually, not computationally, and is therefore qualitative in nature. Both the DNA and the protein were treated as rigid bodies, and no energy minimization was performed. Two possible RTP–DNA docked arrangements were examined for idealness of fit: one in which the β2/β3 ribbons are positioned in the major groove, and the other in which the β-ribbons are positioned in the minor groove. As predicted, in both arrangements, the register of the β-ribbons and α3 helices with successive DNA grooves is ideal. Less ideal is the orientation of α3 with respect to the groove direction. The model requires that the α-helix straddle the groove rather than penetrate it, and this favors interaction of the α-helix with the major groove, at which steric contact is less severe. This places the β-ribbons in the minor groove, and their relative orientations are perfect.

The final docked model of the RTP–DNA complex is shown in Figure 6A. The structures of several protein–DNA complexes have shown that the DNA can be considerably distorted from its standard B conformation, and the model is likely to differ considerably from the actual structure. However, it is a useful basis for further experiments, and it does serve to demonstrate the main features of the protein. As predicted, the protein spans a minimal length of 18 bp along the DNA. The long axis of the protein and that of the DNA are skewed by some 15°, which allows the α3 helices to fit reasonably into the major groove at an angle of 45°. They are close enough to allow surface residues of α3 to "read" the DNA sequence, and there are many candidates for this role (Figure 6B). The interactions of the β-ribbon with the minor grooves appear to be mainly nonspecific since β2 and β3 are heavily populated with

basic residues (see Figure 3A; Figure 6B). However, we have clearly shown that the entire 20-bp DNA sequence is recognized (Mehta et al., 1992), and reading side chains are required in the β-ribbon if our model is correct. The N-termini of RTP are perfectly positioned to read the central minor groove and to interact nonspecifically at their distal ends, at which basic residues predominate (see Figure 3A). The ends are disordered, which would allow them to wrap around the DNA in the complex. Preliminary mutagenesis studies confirm the importance of the N-terminus for binding. To date, 6 out of 9 mutations that have been either selected from randomly mutagenized *rtp* DNA or obtained by site-directed mutagenesis on the basis of reducing the binding of RTP to cognate DNA are located in residues 1–16 (unpublished data).

To check the model for general electrostatic complementarity, the program GRASP (Nicholls and Honig, 1993) was used to generate the charge distribution surface of RTP. Such representations have proven useful in analyzing other protein–DNA complexes (Kong et al., 1992; Sharp, 1994). As shown in Figure 7, the results are quite conclusive. The relevant surface of RTP is highly positively charged and ideal for associating with the negatively charged DNA. Elsewhere on the protein, the charge distribution is effectively random.

RTP–Helicase Interactions

Two alternative mechanisms have been proposed to account for the polar contrahelicase activity of both RTP and the E. coli ter. One mechanism postulates that the terminator proteins form a unique nucleoprotein structure with their cognate DNA that stops helicase-catalyzed DNA unwinding and fork movement, without the occurrence of any specific helicase-terminator protein interaction (Lee and Kornberg, 1992; Gottlieb et al., 1992). We favor the alternative mechanism in which the bound terminator protein presents a specific inhibitory surface to the helicase (Khatri et al., 1989; Natarajan et al., 1993). Implicit in this model is the notion that the terminator proteins would only block replication helicases involved in normal Cairns-type replication, but not those helicases (such as helicases I and II) that are involved in DNA repair and conjugative transfer. Experiments in our laboratory and by others have shown this to be the case (Khatri et al., 1989; Bedrosian and Bastia, 1991; Hiasa and Marians, 1992).

Having produced a model of the RTP–DNA interaction, it is pertinent to ask whether the protein has any surface features that could mediate its interaction with the approaching replication fork. From the model, the most likely region is the exposed surface of the 3-stranded β-pleated sheet, which points down the DNA axis. This surface does indeed contain a distinct hydrophobic patch that could mediate protein–protein interactions (see Figure 3A; see Figure 5B). This suggestion is supported by a second region immediately adjacent to the patch that has a strong similarity to the DnaB initiator protein of B. subtilis (see Figure 3A; see Figure 5B). This similarity was discovered by Kralicek et al. (1991) and spans a 33-residue stretch with 47% identity. It includes amino acids 17–49 and encompasses α1–β1–α2. DnaB is a 55-kDa protein that is responsible for both the membrane attachment of the replication origin of the B. subtilis chromosome and the initiation of replication (Sueoka and Quinn, 1968; Hoshino et al., 1987; Sato et al., 1991).

Although RTP and DnaB have opposite roles in DNA replication, similar functionalities might be needed to accomplish their respective cellular tasks. We suggest that the common requirement is the need to interact with the replicative helicase, which is involved in both the initiation and termination phases of DNA replication. This was 1 of the 3 possible roles that were originally ascribed to this region of homology (Kralicek et al., 1991). The others were DNA binding and an attachment site to a replication apparatus. DNA binding was proposed because the sequence has features that are present in the helix-turn-helix motif. The sequence does form an approximate helix-turn-helix structure in RTP (see Figure 3), but is unlikely to bind DNA owing to its inappropriate orientation. The second possibility cannot be disproven and relates to the observation that the origin and terminus of the B. subtilis chromosome are bound to a common replication apparatus, perhaps a factor within the cellular membrane (Sueoka and Quinn, 1968).

Discussion

Our model for the RTP–DNA interaction suggests that the protein uses three structural features that have been observed in other DNA-binding molecules: a recognition α-helix that penetrates the major groove, antiparallel β-strands that associate with the minor groove, and a flexible N-terminal arm that wraps around the DNA via nonspecific ionic interactions. The first has been observed in many proteins, notably the helix-turn-helix family, and the proposed interaction in RTP resembles that in the CAP–DNA costructure (Schultz et al., 1991). The second is a feature of the HU/integration host factor family of molecules, in which an antiparallel β-ribbon can mediate both specific and nonspecific recognition of DNA (White et al., 1988; Yang and Nash, 1989). It is also a feature of the TATA-binding protein (Kim et al., 1993a, 1993b). Finally, the λ repressor has a positively charged, disordered N-terminal arm that wraps around the DNA and stabilizes the binding (Pabo et al., 1982).

Recent experiments by Langley et al. (1993) and in our laboratory using the RTP/E. coli surrogate system (Kaul et al., 1994; Sahoo et al., 1994) have extended the earlier in vivo observations of Carrigan et al. (1991) and Smith and Wake (1992). In brief, the two RTP molecules bound within each inverted repeat have different affinities for their targets: the first binds tightly and efficiently to one of the repeats (B), but the second will only bind to the other repeat (A) if the first is present. That is, the binding of two RTP molecules is a cooperative process, and the targets are referred to as core (B) and auxiliary (A) sequences to reflect this (Figure 1). This particular arrangement is crucial to polar fork arrest. The binding of both dimers within an inverted repeat is necessary to inhibit effectively passage of the helicase. Furthermore, one core or two tandem cores are insufficient to elicit helicase inhibition and fork

arrest. Thus, the natural complex has important structural properties related to protein–DNA and protein–protein interactions. Some of these features can be addressed by the apostructure of RTP.

As regards the cooperativity, we and others have previously noted that the adjacent RTP target sites within the IR must overlap by several base pairs if each site is 18–20 bp in length (Mehta et al., 1992; Langley et al., 1993). In our DNA binding model, RTP does indeed cover 18–20 bp, and the interaction between adjacent dimers would occur through the flexible loops at the end of the β2/β3 ribbon. There are numerous charged residues within or near the loop that could facilitate such a contact. Most notably, Glu-78 and Lys-81 are unable to form a salt bridge in the monomer, but they are ideally situated to do so across adjacent loops to form two stabilizing salt bridges. A similar type of interaction between the ends of β-ribbons has been proposed to stabilize a multiprotein complex in HU (Tanaka et al., 1984).

Functionally, the polarity of the RTP–DNA complex must result from the different affinities of the two adjacent binding sites and the protein–protein interaction. A simple model is that a replication fork approaching the low affinity side would simply strip off the bound RTP together with its neighbor, whereas a fork approaching the tightly bound RTP would be unable to do so (Sahoo et al., 1994). However, this cannot be the whole explanation because a single RTP bound at the core sequence cannot arrest the fork (Smith and Wake, 1992; Sahoo et al., 1994). We suggest that the complex is structurally asymmetrical in that it "hides" the surface that we propose interacts with DnaB on one side, but makes it accessible on the other side. It is worth noting in this respect that the recognition sequences are extremely A/T-rich and are therefore amenable to distortion or overwinding by compression of the minor groove (Drew and Travers, 1984; Koudelka et al., 1987). As regards the different affinities of the two sites, we have shown (Sahoo et al., 1994) that RTP contacts a pair of guanines that are symmetrically disposed on each strand within the core sequence (Figure 1). Each is 5 bp from the pseudodyad and would therefore interact with helix α3 in our model. In the auxiliary sequence (Figure 1), only one pair is present, which might result in weaker binding of RTP.

We are currently performing additional structural and biochemical experiments to elucidate the mechanism of RTP. Cocrystallization trials have been initiated using the IRIB sequence and variants thereof that have been shown to bind RTP in vitro. Site-directed mutagenesis studies are also underway to investigate the sites on RTP that we suggest are involved in DNA binding, RTP–DnaB interaction, and RTP–RTP cooperativity. We hope to understand the molecular basis of RTP function and prokaryotic replication termination in the near future.

Experimental Procedures

Cells and Strains

The gene encoding B. subtilis RTP was originally cloned into the plasmid pWS46 and overexpressed in E. coli TG-1 cells (Lewis et al., 1990; Mehta et al., 1992). It was decided for two reasons to introduce the RTP gene into the T7 expression system (Studier et al., 1990). First, it should produce higher levels of expression, which would facilitate the structural analysis. Second, it would allow for the incorporation of semet into RTP for the crystallographic analysis. The RTP gene was PCR amplified from pWS46, and NdeI and BamHI sites were simultaneously incorporated at the 5′ and 3′ ends via appropriate PCR primers. The amplified gene was cloned directly into the NdeI and BamHI sites of the vector pET-13A, which provides kanamycin resistance as a selectable marker (Studier et al., 1990). For normal overexpression, the plasmid was transformed into BL21(DE3) cells (Studier et al., 1990). For producing semet-substituted protein, the plasmid was transformed into B834(DE3) cells, which are auxotrophic for methionine. During the PCR amplification, a point mutation (A96T) was introduced into the *rtp* gene, which created a mutant. The resulting protein was very unstable, and the point mutation was repaired by M13 mutagenesis.

For normal protein samples, the BL21(DE3) cells were grown at 37°C in an environmental shaker using LB broth as the growth medium. When the optical density reached 0.7, the cells were induced with 0.4 mM isopropyl-β-D-thiogalactopyranoside (IPTG). After induction (3 hr), the cells were harvested by centrifugation, and the RTP was purified as previously described (Mehta et al., 1992). Typical yields were 5 mg per liter of cells. For expressing the semet-substituted protein, it was necessary to use the following defined medium (per liter); 12 g of Na_2HPO_4, 6 g of KH_2PO_4, 2 g of NH_4Cl, 1 g of NaCl, 4 g of dextrose, 40 mg of kanamycin, 1 mg of biotin, 1 mg of choline chloride, 1 mg of folic acid, 1 mg of niacinamide, 1 mg of D-pantothenate, 1 mg of pyridoxal, 0.1 mg of riboflavin, 5 mg of thiamine, 2 mM $MgSO_4$, 1 μM $FeCl_3$, 0.2 mM $CaCl_2$, 40 mg/l of each amino acid (excluding methionine), and 60 mg/l semet. It was first necessary to acclimate the cells to this medium. The B834(DE3) cells were first grown to turbidity in this medium containing 100% methionine, and this culture was sequentially diluted into media containing 50% and 100% semet. The last culture was used to inoculate a second 2-ml culture containing 100% semet, and this culture was finally used to inoculate a 4-l culture. This was grown and induced as described above, with the notable difference that it took approximately three times longer to reach an appropriate optical density for induction (15 hr as opposed to 5 hr for the BL21(DE3) cells).

Crystallization

Crystals of RTP and semet-substituted RTP were grown in 20% (w/v) PEG 2000 buffered with 0.125 M MES (pH 6.0), as described previously (Mehta et al., 1992). Both forms of the protein crystallize in space group C2 (a = 76.7 Å, b = 52.7 Å, c = 70.4 Å, and β = 90°), with a dimer in the asymmetric unit. The crystals have a varying morphology, often growing as large monoclinic plates measuring 0.4–0.9 mm in the longest dimension. They diffract strongly to 1.9–2.2 Å, depending on the quality of the individual crystal and are stable in the X-ray beam for up to 72 hr. The crystals are stabilized in 30% (w/v) PEG 2000 buffered with 0.25 M MES (pH 6.0).

X-Ray Data Collection and Processing

Data were collected at room temperature by the oscillation method (Wonacott, 1977) on a Rigaku RAXIS II image plate system mounted on a Rigaku RU300 rotating anode X-ray generator (Molecular Structure Corporation) operating at 40 kV and 80 mA. The small size of the unit cell allowed for the collection of relatively large oscillation ranges (3.5°–4.0°), with minimal reflection overlap. The background radiation with these ranges produced no obvious reduction in the quality of the data. Typical crystal-to-detector distances and exposure times were 130 mm and 10 min/degree. These parameters allowed for an almost complete 2.6 Å data set to be collected from a single plate-like crystal in 36 hr. Data processing and reduction were carried out with the RAXIS II software. The native data used in the structure solution represents an amalgam of three individual data sets that were merged to give a high-quality data set, which is 100% complete to 2.6 Å. Derivative data sets were collected in an equivalent manner. The semet-substituted RTP (SEMET) crystals were perfectly isomorphous with native crystals and had an equivalent lifetime in the X-ray beam. The two conventional derivative crystals deteriorated in the beam in approximately 24 hr. Since no significant anomalous signal could be detected in the derivative data, Bijvoet pairs were merged. Statistics for both native and derivative data are given in Table 1.

Table 1. Statistics for Data and Derivatives

Parameters	Native	SEMET	EMTSA	PTCL4
Number of crystals	3	1	1	1
Concentration (mM)			0.7	1
Soaking time (hr)			12	6
Resolution (Å)	2.6	2.6	2.6	2.6
Measured reflections	86,765	33,061	17,960	20,998
Unique reflections	8,781	8,655	7,215	7,708
Completion (%)	99.7	98.9	82.1	85.2
R merge[a] (%)	8.04	4.46	5.28	5.13
Mean isomorphous difference[b] (%)		9.1	11.2	11.8

[a] $\Sigma_h\Sigma_i|(I_{h,i}-I_h)|/\Sigma_h\Sigma I_{h,i}$, where $I_{h,i}$ is the scaled intensity of the i^{th} observation of reflection h, and Ih is the mean value.

[b] $\Sigma|I_{ph}-I_p|/\Sigma I_p$, where I_{ph} and I_p are the scaled derivative and native intensities, respectively.

Table 2. Phasing Data for RTP Heavy Atoms

Heavy Atom Parameters	SEMET	EMTSA	PTCL4
Rc	47	58	62
Sites	4	3	2
Typical B (Å^2)	40	44	67
	Phasing Power		
Resolution (Å)	SEMET	EMTSA	PTCL4
Over 8.6	2.6	2.7	2.2
8.6–4.6	2.4	2.1	1.8
4.6–3.7	2.0	1.8	1.3
3.7–3.3	1.8	1.7	1.1
3.3–2.8	1.7	1.6	1.0
MFOM	0.30	0.32	0.25

Rc, Cullis R factor for centric reflections; phasing power, mean value of heavy atom structure amplitude divided by residual lack of closure error; and MFOM, mean figure of merit (an overall MFOM of 0.50, increasing to 0.77 after solvent flattening, non crystallographic symmetry averaging, and extension cycles).

Structure Solution

The structure of RTP was solved using the heavy atom multiple isomorphous replacement method. The search for heavy atom derivatives was carried out by the usual methods of soaking and cocrystallization. Heavy atom concentrations of 1 mM were typically used, with soak times of 6–24 hr. The crystals proved to be extremely sensitive to the addition of any heavy atom. Of the more than 25 compounds screened, only 5 of these did not cause pathological changes to the crystals, and only 2 yielded derivatives (ethylmercurithiosalicyclic acid [EMTSA] and potassium tetrachloroplatinate [PTCL4]). This difficulty in obtaining derivatives was overcome by the production and crystallization of the semet-substituted protein.

Difference Patterson maps for the semet derivative showed four strong peaks (7–10 standard deviations above the mean density value) in the y = 0 Harker section, and the positions of the selenium atoms were readily determined by manual inspection. SIR phases were calculated and used to locate the heavy atom sites in the EMTSA and PTCL4 derivatives by cross-difference Fourier maps. These locations were confirmed by difference Patterson maps. The heavy atom parameters were refined, and an initial set of multiple isomorphous replacement phases were calculated from the three derivatives. These were markedly improved by solvent flattening (Wang, 1985) using a calculated solvent content of 47% (Matthews, 1968). The phases were used to generate a 3 Å electron density map in which many features of the molecule, most notably the α-helices, could be recognized. As predicted (Mehta et al., 1992), the asymmetric unit contained two molecules: two independent dimers were superimposed on two of the crystallographic 2-fold axes in the C2 space group. Structural landmarks in the map, notably the two 30-residue α-helices (α4) in a coiled-coil configuration, were used to determine the approximate transformation matrix between the two monomers within the asymmetric unit, which was then refined. The final correlation coefficient between the noncrystallographic symmetry related densities was 0.8. A mask of each molecule was calculated from preliminary α-carbon traces, and the equivalent regions of electron density were averaged (Podjarny et al., 1987). Phase extension was used at this point to assign phases to the approximately 180 reflections not phased by the multiple isomorphous replacement approach. Following this procedure, the electron density map was considerably improved, and the whole process was repeated with a more extensive mask based on a new α-carbon trace. The improved phases also enabled the heavy atom parameters to be refined further, which generated a higher quality electron density map at 2.8 Å for the second averaging cycle. After this cycle, the phases were of sufficient quality to calculate a map for model building. All the procedures described above were performed by the PHASES package (Furey and Swaminathan, 1990). All relevant statistics are shown in Table 2.

Model Building

All model building was performed on an Evans and Sutherland ESV workstation using the O program (Jones et al., 1991). The electron density was easily interpretable in both molecules of the asymmetric unit, apart from two loop regions and the N-termini. Both loop regions became interpretable after one round of phase combination (Hendrickson and Lattman, 1970), but the N-termini remained invisible.

Model Refinement

The atomic model, consisting of both independent monomers, was refined against native data in three stages using the program X-PLOR (Brünger, 1988). To monitor progress of the refinement and to guard against overfitting of the model, approximately 10% of the data in each resolution shell was partitioned into a test set and was used to calculate an R_{free} value (Brünger, 1992). Each refinement cycle consisted of 140 steps of Powell minimization, followed by one round of simulated annealing refinement using initial and final temperatures of 3000 K and 300 K, respectively, and 20 cycles of individual restrained B factor refinement. Each monomer was treated independently during the refinement process. Full electrostatic calculations, with the standard cutoff, were included at each step. The structures of both monomers were examined at the end of each cycle with (2Fo-Fc) and (Fo-Fc) maps, using phases calculated from the model. Only minor refitting was necessary, primarily in the ill-defined loop and turn regions previously mentioned. The first refinement cycle utilized data in a range from 15–2.8 Å with a 2σ cutoff. The (2Fo-Fc) map calculated after this cycle revealed the density for residues 7–9 in both monomers, and these residues were built into the model. The second cycle used the more restricted resolution range of 6.0–2.6 Å, again with a 2σ cutoff. The third and final cycle used data from 6.0–2.6 Å, with a 3σ cutoff. The native data were of sufficient quality that a 2σ cutoff excludes less than 1% of the data, while a 3σ cutoff excludes less than 3%. The final model has R and R_{free} factors of 19.3% and 31.6%, respectively. It lacks the N-terminal 6 amino acids for which no interpretable density can be located, and solvent molecules have yet to be included.

Acknowledgments

Correspondence should be addressed to D. B. and S. W. W. We are particularly grateful to Dr. R. G. Wake for providing the overexpressor plasmid of B. subtilis RTP, and we also acknowledge the invaluable assistance of Dr. I. Patel in performing the M13 mutagenesis. We also thank S. Porter for technical assistance, M. Finnin and C. Davies for many useful discussions, and F. William Studier for providing the B834(DE3) cells for incorporating semet. This work was supported by National Institutes of Health grant GM49264 (to D. B. and S. W. W.) and also by a generous award from the Rippel Foundation.

Received October 5, 1994; revised December 2, 1994.

References

Bastia, D., Germino, J., Crosa, J. H., and Ram, J. (1981). The nucleotide sequence surrounding the replication terminus of R6K. Proc. Natl. Acad. Sci. USA *78*, 2095–2099.

Bedrosian, C. L., and Bastia, D. (1991). *Escherichia coli* replication terminator protein impedes simian virus 40 (SV40) DNA replication fork movement and SV40 large tumor antigen helicase activity *in vitro* at a prokaryotic terminus sequence. Proc. Natl. Acad. Sci USA *88*, 2618–2622.

Brünger, A. T. (1988). X-PLOR: A System for X-Ray Crystallography and NMR (New Haven, Connecticut: Yale University Press).

Brünger, A. T. (1992). Free R value: a novel statistical quantity for assessing the accuracy of crystal structures. Nature *355*, 472–475.

Burley, S. K., and Petsko, G. A. (1985). Aromatic–aromatic interaction: a mechanism of protein structure stabilization. Science *229*, 23–28.

Carrigan, C. M., Pack, R. A., Smith, M. T., and Wake, R. G. (1991). Normal *terC*-region of the *Bacillus subtilis* chromosome acts in a polar manner to arrest the clockwise replication fork. J. Mol. Biol. *222*, 197–207.

Crick, F. H. C. (1953). The packing of α-helices: simple coiled-coils. Acta Crystallogr. *6*, 689–697.

Cusack, S., Berthet-Colominas, C., Hartlein, M., Nassar, N., and Leberman, R. (1990). A second class of synthetase structure revealed by X-ray analysis of *Escherichia coli* seryl-tRNA synthetase at 2.5 Å. Nature *347*, 249–255.

Drew, H. R., and Travers, A. A. (1984). DNA structural variations in the E. coli *tyrT* promoter. Cell *37*, 491–502.

Furey, W., and Swaminathan, S. (1990). PHASES. Am. Crystallogr. Assoc. Annu. Mtg. Program Abstr. *18*, 73.

Gottlieb, P. A., Wu, S., Zhang, X., Tecklenburg, M., Kuempel, P., and Hill, T. M. (1992). Equilibrium, kinetic, and footprinting studies of the Tus-Ter protein–DNA interaction. J. Biol. Chem. *267*, 7434–7443.

Hendrickson, W. A., and Lattman, E. E. (1970). Representation of phase probability distributions for simplified combination of independent phase information. Acta Crystallogr. *B26*, 136–143.

Hiasa, H., and Marians, K. J. (1992). Differential inhibition of the DNA translocation and DNA unwinding activities of DNA helices by the *Escherichia coli* Tus protein. J. Biol. Chem. *267*, 11379–11385.

Hoshino, T., McKenzie, T., Schmidt, S., Tanaka, T., and Sueoka, N. (1987). Nucleotide sequence of *Bacillus subtilis* DnaB: a gene essential for DNA replication and membrane attachment. Proc. Natl. Acad. Sci. USA *84*, 653–657.

Jones, T. A., Zou, J. Y., Cowan, S. W., and Kjeldgaard, M. (1991). Improved methods for building protein models in electron density maps and the location of errors in these models. Acta Crystallogr. *A47*, 110–119.

Kaul, S., Mohanty, B., Sahoo, T., Patel, I., Khan, S. A., and Bastia, D. (1994). The replication terminator protein of the gram positive bacterium *B. subtilis* functions as a polar contrahelicase in gram negative *E. coli*. Proc. Natl. Acad. Sci. USA *91*, 11143–11147.

Khatri, G. S., MacAllister, T., Sista, P. R., and Bastia, D. (1989). The replication terminator protein of E. coli is a DNA sequence-specific contra-helicase. Cell *59*, 667–674.

Kim, J. L., Nikolov, D. B., and Burley, S. K. (1993a). Co-crystal structure of TBP recognizing the minor groove of a TATA element. Nature *365*, 520–527.

Kim, Y., Geiger, J. H., Hahn, S., and Sigler, P. B. (1993b). Crystal structure of a yeast TBP/TATA-box complex. Nature *365*, 512–520.

Kong, X.-P., Onrust, R., O'Donnell, M., and Kuriyan, J. (1992). Three-dimensional structure of the β subunit of E. coli DNA polymerase III holoenzyme: a sliding DNA clamp. Cell *69*, 425–437.

Koudelka, G. B., Harrison, S. C., and Ptashne, M. (1987). Effect of non-contacted bases on the affinity of 434 operator for 434 repressor and Cro. Nature *326*, 886–888.

Kralicek, A. V., Day, A. J., Wake, R. G., and King, G. F. (1991). A sequence similarity between proteins involved in initiation and termination of bacterial chromosome replication. Biochem. J. *275*, 823.

Kralicek, A. V., Vesper, N. A., Ralston, G. B., Wake, R. G., and King, G. F. (1993). Symmetry and secondary structure of the replication terminator protein of *Bacillus subtilis*: sedimentation equilibrium and circular dichroic, infrared, and NMR spectroscopic studies. Biochemistry *32*, 10216–10223.

Kraulis, P. J. (1991). MOLSCRIPT: a program to produce both detailed and schematic plots of protein structures. J. Appl. Crystallogr. *24*, 946–950.

Kuempel, P. L., Duerr, S. A., and Seeley, N. R. (1977). Terminus region of the chromosome in *Escherichia coli* inhibits replication forks. Proc. Natl. Acad. Sci. USA *74*, 3927–3931.

Langley, D. B., Smith, M. T., Lewis, P. J. and Wake, R. G. (1993). Protein–nucleoside contacts in the interaction between the replication terminator protein of *Bacillus subtilis* and the DNA terminator. Mol. Microbiol. *10*, 771–779.

Lee, B., and Richards, F. M. (1971). The interpolation of protein structures: estimation of static accessibility. J. Mol. Biol. *55*, 379–400.

Lee, E. H., and Kornberg, A. (1992). Features of replication fork blockage by the *E. coli* terminus binding protein. J. Biol. Chem. *267*, 8778–8784.

Levitt, M., and Chothia, C. (1976). Structural patterns in globular proteins. Nature *261*, 552–558.

Lewis, P. J., and Wake, R. G. (1991). Termination of chromosomal replication in *Bacillus subtilis*. Res. Microbiol. *142*, 893–900.

Lewis, P. J., Smith, M. T., and Wake, R. G. (1989). DNA and protein sequence conservation at the replication terminus in *Bacillus subtilis* 168 and W23. J. Bacteriol. *171*, 3564–3567.

Lewis, P. J., Ralston, G. B., Christopherson, R. I., and Wake, R. G. (1990). Identification of the replication terminator protein binding sites in the terminus regions of the *Bacillus subtilis* chromosome and the stoichiometry of binding. J. Mol. Biol. *244*, 73–84.

Luthy, R., Bowie, J. U., and Eisenberg, D. (1992). Assessment of protein models with three-dimensional profiles. Nature *356*, 83–85.

MacAllister, T., Khatri, G. S., and Bastia, D. (1990). Sequence-specific and polarized replication termination *in vitro*: complementation of extracts of tus$^-$ *E. coli* by purified ter protein and analysis of termination intermediates. Proc. Natl. Acad. Sci. USA *72*, 2905–2909.

Matthews, B. W. (1968). Solvent content of protein crystals. J. Mol. Biol. *33*, 491–497.

Mehta, P. P., Bussiere, D. E., Hoffman, D. W., Bastia, D., and White, S. W. (1992). Crystallization and preliminary structural analysis of the replication terminator protein of *Bacillus subtilis*. J. Biol. Chem. *267*, 18885–18889.

Natarajan, S., Kaul, S., Miron, A., and Bastia, D. (1993). A 27 kd protein of E. coli promotes antitermination of replication in vitro at a sequence-specific replication terminus. Cell *72*, 113–120.

Nicholls, A., and Honig, B. (1993). GRASP (New York: Columbia University).

Oas, T. G., and Endow, S. A. (1994). Springs and hinges: dynamic coiled-coils and discontinuities. Trends Biochem. Sci. *19*, 51–54.

Ollis, D. L., and White, S. W. (1987). Structural basis of protein–nucleic acid interactions. Chem. Rev. *87*, 981–995.

O'Shea, E. K., Klemm, J. D., Kim, P. S., and Alber, T. (1991). X-ray structure of the GCN4 leucine zipper, a two-stranded, parallel coiled coil. Nature *254*, 539–544.

Pabo, C. O., and Lewis, M. (1982). The operator-binding domain of lambda repressor structure and DNA recognition. Nature *298*, 443–447.

Pabo, C. O., Krovatin, K., Jeffrey, A., and Sauer, R. T. (1982). The N-terminal arms of lambda repressor wrap around the operator DNA. Nature *298*, 441–443.

Pathak, D., and Sigler, P. B. (1992). Updating structure–function relationships in the bZip family of transcription factors. Curr. Opin. Struct. Biol. *2*, 116–123.

Podjarny, A. D., Bhat, T. N., and Zwick, M. (1987). Improving crystallographic macromolecular images: the real-space approach. Annu. Rev. Biophys. Biophys. Chem. *16*, 351–373.

Richards, F. M. (1977). Areas, volumes, packing, and protein structure. Annu. Rev. Biophys. Bioeng. *6*, 151–176.

Sahoo, T., Mohanty, B., Patel, I., and Bastia, D. (1995). Termination of DNA replication *in vitro*: requirement for specific stereochemical interactions between two dimers of the replication terminator protein and the terminator site for eliciting polar contrahelicase activity and fork impedance. EMBO J. *14*, in press.

Sato, Y., McCollum, M., McKenzie, T., Laffan, J., Zuberi, A., and Sueoka, N. (1991). *In vitro* type II binding of chromosomal DNA to membrane in *Bacillus subtilis*. J. Bacteriol. *173*, 7732–7735.

Scholtz, J. M., Quian, H., Robbins, V. H., and Baldwin, R. L. (1993). The energetics of ion-pair and hydrogen-bonding interactions in a helical peptide. Biochemistry *32*, 9668–9676.

Schultz, S. C., Shields, G. C., and Steitz, T. A. (1991). Crystal structure of a CAP–DNA complex: the DNA is bent by 90°. Science *253*, 1001–1007.

Sharp, K. A. (1994). Electrostatic interaction in macromolecules. Curr. Opin. Struct. Biol. *4*, 234–239.

Sista, P., Hutchison, C., and Bastia, D. (1991). DNA–protein interaction at the replication termini of plasmid R6K. Genes Dev. *5*, 74–82.

Smith, M. T., and Wake, R. G. (1992). Definition and polarity of action of DNA replication terminators in *Bacillus subtilis*. J. Mol. Biol. *227*, 648–657.

Steitz, T. A. (1990). Structural studies of protein–nucleic acid interaction: the sources of sequence-specific binding. Q. Rev. Biophys. *23*, 205–280.

Studier, F. W., Rosenberg, A. H., Dunn, J. J., and Dubendorff, J. W. (1990). Use of T7 RNA polymerase to direct the expression of cloned genes. Meth. Enzymol. *185*, 60–89.

Sueoka, N., and Quinn, W. G. (1968). Membrane attachment of the chromosome replication origin in *Bacillus subtilis*. Cold Spring Harb. Symp. Quant. Biol. *33*, 695–705.

Tanaka, I., Appelt, K., Dijk, J., White, S. W., and Wilson, K. S. (1984). 3-Å resolution structure of a protein with histone-like properties in prokaryotes. Nature *310*, 376–381.

Wang, B. C. (1985). Resolution of phase ambiguity in macromolecular crystallography. Meth. Enzymol. *115*, 90–112.

Weiss, A. S., and Wake, R. G. (1984). A unique DNA intermediate associated with termination of chromosome replication in Bacillus subtilis. Cell *39*, 683–689.

White, S. W., Appelt, K., Wilson, K. S., and Tanaka, I. (1988). A protein structural motif that bends DNA. Proteins: Struct. Func. Genet. *5*, 281–288.

Wonacott, A. J. (1977). Geometry of the rotation method. In The Rotation Method in Crystallography, U. W. Arndt and A. J. Wonacott, eds. (Oxford: North-Holland Publishing), pp. 75–105.

Yang, C.-C., and Nash, H. A. (1989). The interaction of E. coli IHF protein with its specific binding sites. Cell *57*, 869–880.